Shannon capacities and error-correction codes for optical atmospheric turbulent channels

Jaime A. Anguita, Ivan B. Djordjevic, Mark A. Neifeld, and Bane V. Vasic

Department of Electrical and Computer Engineering, The University of Arizona, 1230 E. Speedway Boulevard, Tucson, Arizona 85721

janguita@ece.arizona.edu

RECEIVED 18 APRIL 2005; REVISED 24 JUNE 2005;
ACCEPTED 25 JULY 2005; PUBLISHED 24 AUGUST 2005

The propagation of an ON–OFF keying modulated optical signal through an optical atmospheric turbulent channel is considered. The intensity fluctuations of the signal observed at the receiver are modeled using a gamma–gamma distribution. The capacity of this channel is determined for a wide range of turbulence conditions. For a zero inner scale, the capacity decreases monotonically as the turbulence strengthens. For non-zero inner scale, the capacity is not monotonic with turbulence strength. Two error-correction schemes, based on low-density parity-check (LDPC) codes, are investigated as a means to improve the bit-error rate (BER) performance of the system. Very large coding gains—ranging from 5.5 to 14 dB, depending on the turbulence conditions—are obtained by these LDPC codes compared with Reed–Solomon error-correction codes of similar rates and lengths.

OCIS codes: 010.1330, 060.4510.

1. Introduction

The atmospheric free-space channel is a natural medium for outdoor optical wireless communication and has generated significant research attention in the past 10 years as a complement to radio-frequency (RF) links. The free-space optical (FSO) atmospheric channel has a wide bandwidth and may support many more users than an RF channel. Most optical wireless links are based on intensity modulation with direct detection, the same technique that is used for state of the art fiber-optics communications. The availability of the optical components used in fiber optics makes outdoor optical links a cost-effective solution for high-rate voice and data communications [1, 2]. Communication in a FSO channel is achieved by a point-to-point connection of two optical transceivers in line of sight. An optical wave propagating through the air experiences random variations in phase and amplitude due to the effects of turbulence. This turbulence is caused by fluctuations in the refractive index of the medium as the latter experiences temperature gradients due to solar heating and wind [3].

To design a high-performance communication link for the atmospheric FSO channel, it is of great importance to characterize the channel from the perspective of information theory. In this paper we study the Shannon capacity of the atmospheric FSO link using an accurate scintillation model based on the gamma–gamma probability distribution function to predict the fluctuation of the intensity signal [4, 5]. This statistical representation not only fits the channel scintillation accurately, but its parameters can be related to the physical conditions of turbulence by a scintillation model proposed by Andrews *et al.* [6]. Previous studies have considered the use of the lognormal distribution [7], but its validity is limited to very weak turbulence [4, 6]. To estimate the channel capacity, a system based on ON–OFF keying (OOK) modulation and a point detector is studied. The noise in the receiver electronics is modeled as additive white Gaussian noise (AWGN). A broad range

in turbulence strength—from the weak turbulence regime through the saturation regime—is considered. We show that atmospheric turbulence reduces the channel capacity, and the latter reaches an asymptotic limit in the saturation regime.

The probability of bit error under several turbulence conditions is determined using Monte Carlo simulations. We demonstrate that appropriate forward error correction (FEC) codes can provide a significant coding gain in signal-to-noise ratio (SNR) with respect to an uncoded system. In particular, we present two error correction systems based on low-density parity-check (LDPC) codes: (i) LDPC codes designed using the MacNeish–Mann theorem and (ii) block-circulant codes; both codes we proposed recently for fiber-optics communications [8, 9]. The codes have quasi-cyclic structure of parity-check matrix, high code rate, low encoder and decoder complexity, and excellent error correction capabilities. For more details on LDPC codes, the interested reader is referred to Refs. [8–11]. The bit-error rate (BER) performance of LDPC codes are compared against Reed–Solomon (RS) codes of similar rates and lengths. The LDPC codes provide significant coding gain improvement compared with standard RS codes, ranging from about 6 dB to about 14 dB, depending on the turbulence strength.

The paper is organized as follows. A brief description of an FSO communication system is given in Section 2. In Section 3 we describe the statistical model for the intensity variations caused by atmospheric turbulence. The zero and the nonzero inner scale models are presented in subsections *A* and *B*, respectively. In Section 4 we present the computation of channel capacities based on the statistical model and we explain the implications on high-bit-rate communication links. In Section 5 we present a comparison of BER performances of the FEC codes and the uncoded link for some channels. In Section 6 we summarize our work and provide our conclusions.

2. System Description

A basic point-to-point FSO system, shown in Fig. 1, consists of a transmitter, a propagation path, and a receiver. The typical optical transmitter includes a light source (i.e., a semiconductor laser of high launch power and wide bandwidth) and a telescope assembly designed using either lenses or a parabolic mirror. An electrical data stream carrying the network traffic modulates the light source. The modulated beam is projected toward the receiver. At the receiver, an optical system collects the light, and focuses it onto a detector, which delivers an electrical signal proportional to the incoming optical signal. The receiver commonly employs the transimpedance design, a good compromise between the noise and bandwidth. A preamplified PIN photodiode or an avalanche photodiode is typically used as optical detector. During propagation through the air, the optical beam experiences amplitude and phase variations caused by scattering, refraction caused by atmospheric turbulence, absorption, and building sway. The receiver electronics introduce noise, making the detection of the binary data subject to errors. If error correction codes are used, the input electrical data stream is encoded before transmission and later decoded at the receiver after the optical-to-electrical conversion.

3. Atmospheric Turbulent Channel Modeling

A commonly used turbulence model assumes that the variations of the medium can be understood as individual cells of air or eddies of different diameters and refractive indices. In the context of geometrical optics, these eddies may be thought of as lenses that randomly refract the optical wavefront, producing a distorted intensity profile at the receiver of a communication system. The intensity fluctuations are called scintillation, one of the most important factors that limit the performance of an atmospheric FSO communication link. The most widely accepted theory of turbulence is attributed to Kolmogorov [3, 12–14].

This theory assumes that kinetic energy from large turbulent eddies, characterized by the outer scale L_0, is transferred without loss to eddies of decreasing size down to sizes of a few millimeters characterized by the inner scale l_0. The inner scale represents the cell size at which energy is dissipated by viscosity. The refractive index varies randomly across the different turbulent eddies and causes phase and amplitude variations to the wavefront. Turbulence can also cause the random drifts of optical beams—a phenomenon usually referred to as wandering—and can induce beam focusing.

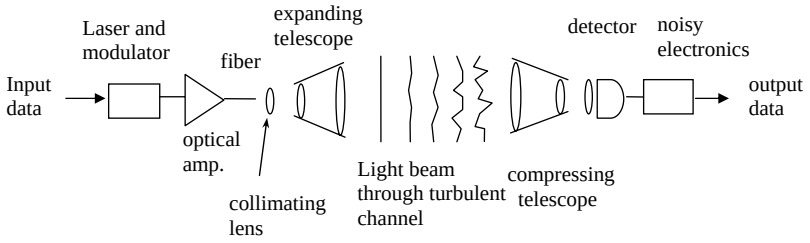

Fig. 1. FSO communication link under study.

Outer scale is assumed to be infinite in this study. We consider zero and nonzero inner scale conditions. Understanding the turbulence effects under zero inner scale is important, as it represents a physical bound for the optical atmospheric channel and as such it has been of interest to researchers [4, 6, 15].

To account for the strength of the turbulence, we use the unitless Rytov variance, given by [3, 13]

$$\sigma_R^2 = 1.23\, C_n^2 k^{7/6} L^{11/6}, \tag{1}$$

where $k = 2\pi/\lambda$ is the wavenumber, λ is the wavelength, L is the propagation distance, and C_n^2 is the refractive index structure parameter, which we assume to be constant for horizontal paths. Although the Rytov variance has been used as an estimate of the intensity variance in week turbulence, we use it here only as an intuitive metric that brings together all the physical operating conditions. Throughout the paper we often refer to σ_R simply as turbulence strength.

To characterize the FSO channel from a communication theory perspective, it is useful to give a statistical representation of the scintillation. The reliability of the communication link can be determined if we use a good probabilistic model for the turbulence. Several probability density functions (PDFs) have been proposed for the intensity variations at the receiver of an optical link [15–20]. Al-Habash *et al.* [4] proposed a statistical model that factorizes the irradiance as the product of two independent random processes each with a Gamma PDF. The PDF of the intensity fluctuation is therefore

$$f(I) = \frac{2(\alpha\beta)^{(\alpha+\beta)/2}}{\Gamma(\alpha)\Gamma(\beta)} I^{(\alpha+\beta)/2-1} K_{\alpha-\beta}\left(2\sqrt{\alpha\beta I}\right), \quad I > 0, \tag{2}$$

where I is the signal intensity, α and β are parameters of the PDF, Γ is the gamma function, and $K_{\alpha-\beta}$ is the modified Bessel function of the second kind of order $\alpha - \beta$.

3.A. *Zero Inner Scale*

The parameters α and β of the PDF that predicts the scintillation experienced by plane waves in the case of $l_0 = 0$, are given by the expressions [4, 12]

$$\alpha = \left(\exp\left[\frac{0.49\sigma_R^2}{\left(1 + 1.11\sigma_R^{12/5}\right)^{7/6}} \right] - 1 \right)^{-1},$$
$$\beta = \left(\exp\left[\frac{0.51\sigma_R^2}{\left(1 + 0.69\sigma_R^{12/5}\right)^{5/6}} \right] - 1 \right)^{-1}, \tag{3}$$

where σ_R^2 is the Rytov variance as given in Eq. (1). This is a very significant result, as the PDF of the intensity fluctuations at the receiver can be predicted from the physical turbulence conditions. The predicted distribution matches very well the distributions obtained from numerical propagation simulations [4, 15]. The predicted gamma–gamma distribution fits even better than the log-normal distribution in the weak turbulence regime. The poorest fit with experiments occurs in the focusing regime, where σ_R is about 2 to 3.

Figure 2 shows the predicted distribution for a few instances of the turbulence strength. For $\sigma_R \ll 1$, the gamma–gamma distribution resembles a log-normal distribution. As the turbulence strength increases the distribution skews towards smaller values of irradiance. The distribution of the intensity fluctuations asymptotically approaches an exponential distribution as σ_R tends to infinity.

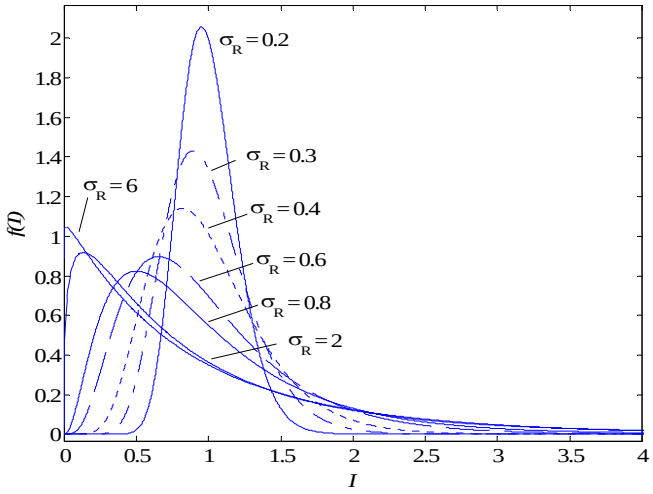

Fig. 2. Distribution of intensity fluctuations for several values of the turbulence strength.

3.B. *Nonzero Inner Scale*

In the presence of non-zero inner scale, the model must be modified to account for the slight change in the power spectrum of the refractive index variations. The PDF model is again a gamma–gamma distribution, but its parameters are now given by [4, 12]

$$\alpha = \left\{ \exp\left[\sigma_{\ln X}^2 \right] - 1 \right\}^{-1}$$
$$\beta = \left\{ \exp\left[\frac{0.51\sigma_P^2}{\left(1 + 0.69\sigma_P^{12/5}\right)^{5/6}} \right] - 1 \right\}^{-1}, \tag{4}$$

where $\sigma^2_{\ln X}$ is given by

$$\sigma^2_{\ln X} = 0.16\sigma_1^2 \left(\frac{\eta_x Q}{\eta_x + Q}\right)^{7/6} \left[1 + 1.75\left(\frac{\eta_x}{\eta_x + Q}\right)^{1/2} - 0.25\left(\frac{\eta_x}{\eta_x + Q}\right)^{7/12}\right], \quad (5)$$

$$\eta_x = \frac{2.61}{1 + 0.45\sigma_1^2 Q^{1/6}}, \quad Q = \frac{10.89L}{kl_0^2}. \quad (6)$$

For the second expression in Eq. (4), σ_P^2 is given by

$$\sigma_P^2 = 3.86\sigma_1^2 \left\{ \left(1 + 1/Q^2\right)^{11/12} \left[\sin\left(\frac{11}{6}\tan^{-1} Q\right) + \frac{1.51}{\left(1 + Q^2\right)^{1/4}} \sin\left(\frac{4}{3}\tan^{-1} Q\right) - \frac{0.27}{\left(1 + Q^2\right)^{7/24}} \sin\left(\frac{5}{4}\tan^{-1} Q\right)\right] - 3.5Q^{-5/6} \right\}. \quad (7)$$

4. Channel Capacity of an Atmospheric FSO Channel

The capacity of a noisy channel relates the SNR of the received signal to the average rate of symbols per channel use that can be recovered with an arbitrarily small probability of error. If we use a binary alphabet, the maximum rate we can achieve is 1 bit/channel use and this limit is realized only for infinite SNR. The channel capacity can also be expressed in terms of bandwidth efficiency (bits/s/Hz) if the frequency response of the channel is known. In most cases the channel capacity can only be achieved by using long error-correction codes. To be able to reduce the BER to an arbitrarily small value at any given SNR, the rate R of the code has to be smaller than the channel capacity C at that SNR [21]. We define $\text{SNR} = \text{E}[I]^2/N_0$, where E[ ] is the expectation operator, I is the received intensity, and N_0 is the electrical noise power.

We are interested in determining the channel capacity of the FSO channel for different turbulence conditions. This can lead to better understanding of the effects of turbulence in a high-bit-rate optical communication system and helps to learn about on which conditions the channel can be more effectively utilized. Some work on capacity estimation has been previously done under weak turbulence by using the lognormal statistical model [7]. We consider the complete range of turbulence strength, from very weak turbulence to the saturation regime. It is intuitively clear that higher turbulence strength will lead to a reduction in channel capacity; however, we seek a quantitative description of this capacity reduction. Below we describe the assumptions under which we determine the channel capacity of the optical atmospheric channel.

4.A. Channel Capacity Calculation

The assumptions made to determine channel capacity are as follows:

(i) The received intensity samples are treated as independent and identically distributed (i.i.d.); that is, the channel is assumed to be uncorrelated. In reality, at high bit rates the channel has temporal correlation and consecutive bits propagate through similar channel conditions [1]. Because of the lack of literature in regard of the temporal statistics in the FSO channel and the difficulty of tractability of multidimensional joint distributions, we consider an i.i.d. case, as it will produce a lower bound in capacity. This approach is valid because temporal correlation can in practice be overcome by means of long interleavers. Hence, this type of correlation does not place a constraint on capacity [22, 23]. For brief periods of time the instantaneous capacity may be reduced or increased due to scintillation. If the bit time is much smaller that the correlation time, the channel can be sensed and this information can be used to improve the detection of further bits, yielding a higher capacity.

However, without the knowledge of the temporal statistics, the receiver uses a symbol-by-symbol detection scheme.

(ii) The marginal distribution of the channel is known. This means that we can determine the turbulence conditions and can predict the parameters of the gamma–gamma distribution. This assumption is sound, as all the physical parameters can be effectively measured.

(iii) We assume an intensity-based OOK modulation scheme and model the noise at the receiver as AWGN.

The statistical channel can be represented by the expression

$$Y = IX + N, \quad I > 0, \tag{8}$$

where Y is the received signal, I is a random variable representing the intensity gain, X is the transmitted binary signal, and N is the noise at the receiver. We assume for simplicity that the responsivity factor of the detector is equal to 1. If a "0" is transmitted, the received signal is given by noise alone. If a "1" is transmitted, the channel will randomly scale the input signal by a factor that follows a gamma–gamma distribution according to the model described above. Channel capacity for a binary-input continuous-output channel is defined as the maximum of the mutual information between X and Y over all input distributions [21]. In this case, the input distribution is binomial. The mutual information for this channel is, therefore,

$$I(Y;X) = \int_0^{\infty} \sum_{x=0}^{1} f_Y(y \mid x) P_X(x) \log_2 \frac{f_Y(y \mid x)}{\sum_{z=0}^{1} f_y(y \mid z) P_X(z)} \mathrm{d}y, \tag{9}$$

where $f_Y(y \mid x)$ is the conditional distribution of the output Y given the input X, and $P_X(x)$ is the probability of $X = x$.

The conditional distribution $f_Y(y \mid x = 0)$ is a zero-mean Gaussian distribution, and $f_Y(y \mid x = 1)$ is the distribution of $I + N$. We determine $f_Y(y \mid x = 1)$ numerically, using the fact that the PDF of the sum of two random variables is the convolution of their PDFs [24]. Because the channel is asymmetric, the input distribution that maximizes the mutual information is no longer $P_X(0) = P_X(1) = 0.5$. In fact the optimal input distribution varies with the turbulence strength and the SNR, and it ranges from about $P_X(0) = 0.56$ for strong turbulence and low SNR to about $P_X(0) = 0.5$ for weak turbulence and high SNR. We determine the capacity C from Eq. (9) using Monte Carlo integration [25].

4.B. *Capacity for Zero Inner Scale*

Table 1 summarizes the turbulence conditions considered and the corresponding distribution parameters for $l_0 = 0$. The final column indicates the variance of the intensity fluctuations, usually referred to as scintillation index. Figure 3 shows the channel capacity for plane waves considering OOK modulation and a point receiver, expressed as bits/channel use versus SNR in decibels. For the sake of a comparison, the capacity of an OOK AWGN channel with the same modulation scheme is also shown. Each curve represents the maximum possible coding rate at which the probability of error can be made arbitrarily small for a given SNR and turbulence strength.

Under weak turbulence the capacity approaches that of a binary AWGN channel as the turbulence strength decreases. We see that as σ_R increases, the capacity decreases. This in turn will result in worse performance of the communication link. Under weak turbulence the capacity decreases more rapidly as σ_R increases, for a given rate. It is interesting to see that beyond the weak turbulence regime ($\sigma_R > 2$), the capacity curves keep shifting to higher SNR values but at smaller steps. For very strong turbulence, capacity curves asymptotically approach a limit. This means that regardless of the propagation distance and

Table 1. Channel Parameters For Capacity Computations for Zero Inner Scale

σ_R	α	β	σ_I^2
0.2	51.91	49.11	0.04
0.4	14.11	12.54	0.156
0.6	7.38	5.86	0.329
0.8	5.23	3.59	0.523
1.0	4.39	2.56	0.706
1.5	4.01	1.61	1.025
2.0	4.34	1.31	1.171
3.0	5.49	1.12	1.242
4.0	6.76	1.06	1.234
5.0	8.05	1.03	1.214
6.0	9.31	1.02	1.194
10.0	14.11	1.0033	1.138

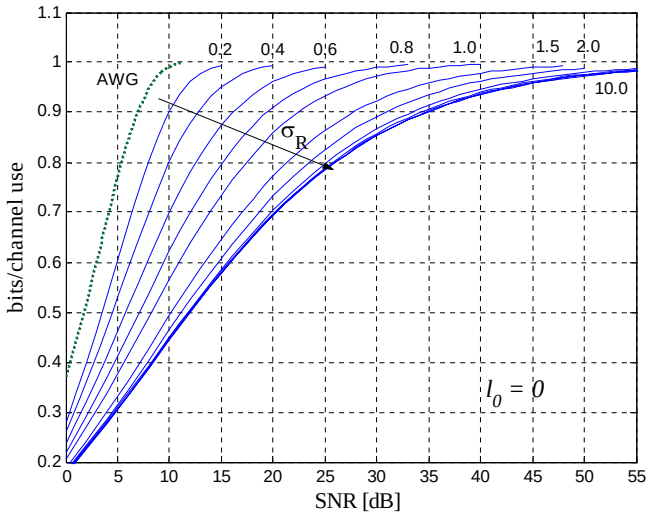

Fig. 3. Capacity of the FSO atmospheric channel using OOK as a function of SNR. The dotted curve is the capacity of an OOK AWGN channel.

turbulence strength, the performance will not drop below this asymptotic limit, assuming that attenuation is compensated.

Another useful way to analyze the capacity is to plot the SNR required to achieve a constant rate (in bits/channel use) as a function of σ_R. This is shown in Fig. 4. For any given rate, the required SNR grows more rapidly for small σ_R, meaning that most of the degradation in capacity occurs in weak turbulence. From the curves of Fig. 4, for fixed SNR, it can be concluded that there exists a monotonic decrease of capacity as turbulence strength σ_R increases. At high rates, we find that the SNR suffers stronger degradation compared with lower rates. We see that at a rate $R = 0.5$ the required SNR is almost constant in strong turbulence ($\sigma_R > 2$). However, at a rate $R = 0.9$, the SNR required increases significantly up to a turbulence strength of about $\sigma_R = 4$. It appears that the power penalty for using higher code rate FEC codes is large. It is worth recalling, however, that FEC codes incur a SNR penalty inversely proportional to the rate. Moreover, for a reasonable throughput, high-rate codes are necessary.

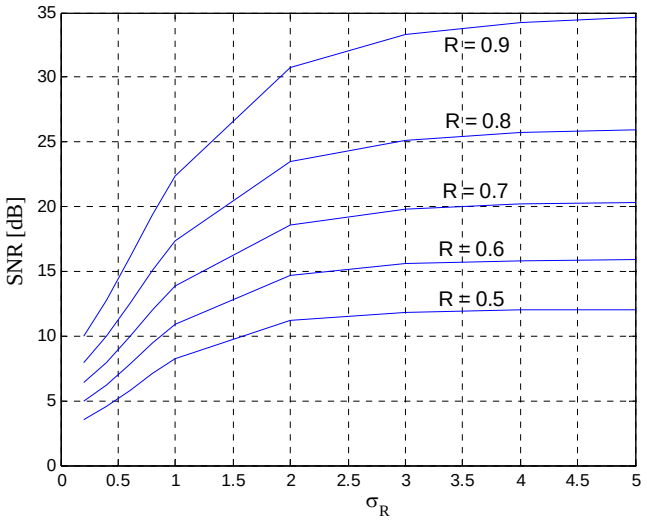

Fig. 4. Required SNR to maintain a constant rate as a function of σ_R.

The curves presented in Figs. 3, 4 are universal; that is, they apply for any combination of propagation length L, wavelength λ, and structure parameter C_n^2, as long as L is much larger than λ, so that the geometrical optics approximation used in deriving Eq. (3) holds. In practice, the refractive index structure parameter C_n^2 varies from about $10^{-17}\,\mathrm{m}^{-2/3}$ for very weak turbulence to about $10^{-12}\,\mathrm{m}^{-2/3}$ for strong turbulence. For instance, a value of $\sigma_R = 1$ can be obtained with $C_n^2 = 8 \times 10^{-14}\,\mathrm{m}^{-2/3}$, $L = 500\,\mathrm{m}$, and $\lambda = 780\,\mathrm{nm}$.

4.C. *Capacity for Nonzero Inner Scale*

For non-zero l_0, the capacity is computed as in the previous section but the parameters of the PDF are predicted according to Eq. (4). Because there is an additional degree of freedom, the capacity cannot be represented by a single set of curves as before. It is convenient to use the parameter Q, defined by Eq. (6), as the free variable as it accounts for propagation distance, inner scale, and wavelength. We present the capacity for three values of Q, namely 200, 32, and 8. Table 2 shows the distribution parameters we consider for $Q = 200$. The values of Q considered above are obtained, for instance, with $L = 592\,\mathrm{m}$, $\lambda = 780\,\mathrm{nm}$, and inner-scale values 2 mm, 5 mm, and 10 mm, respectively. Because σ_R depends on L and λ, the free parameter will be C_n^2. Given the values above, varying σ_R from 0.2 to 10 is equivalent to varying C_n^2 from $2 \times 10^{-15}\,\mathrm{m}^{-2/3}$ to $6 \times 10^{-12}\,\mathrm{m}^{-2/3}$. For smaller values of C_n^2, the curve of capacity is expected to come nearer the capacity of the AWGN channel.

Figures 5, 6, 7 show the capacity curves for $Q = 200$, 32, and 8, respectively. These curves show a similar behavior to that of the zero inner-scale case. There are, however, some noteworthy differences. The capacity curves experience a stronger shift to higher SNR values as Q decreases. In other words, for a given σ_R, capacity decreases as Q decreases. For instance, at $\sigma_R = 1$, a rate 0.8 bits/channel use is achieved at an SNR of 17 dB for $Q = 200$ (Fig. 5), at 21.1 dB for $Q = 32$ (Fig. 6), and at 21.6 dB for $Q = 8$ (Fig. 7). If L, k, and C_n^2 are kept constant, we can conclude that capacity decreases as the inner scale increases.

In the saturation regime $(\sigma_R > 3)$, the capacity is no longer monotonic with σ_R. This is subtle for $Q = 200$ (Fig. 5), but very noticeable at $Q = 8$ (Fig. 7). The insets in Figs. 5, 6, 7 show detailed sections of the capacity curves. Beyond certain σ_R, the curves shift to lower values of SNR. The value at which this occurs depends on Q. This trend is more

Table 2. Channel Parameters For Capacity Computations for $Q = 200$.

σ_R	α	β	σ_I^2
0.2	45.79	41.55	0.0464
0.4	12.87	10.67	0.179
0.6	6.82	5.05	0.374
0.8	4.75	3.14	0.596
1.0	3.83	2.29	0.811
1.5	3.04	1.50	1.214
2.0	2.88	1.25	1.422
3.0	2.98	1.09	1.557
4.0	3.18	1.05	1.571
5.0	3.41	1.03	1.555
6.0	3.62	1.02	1.534
7.0	3.82	1.01	1.512
8.0	4.00	1.006	1.493
9.0	4.17	1.004	1.475
10.0	4.34	1.002	1.459

clearly seen by plotting SNR versus σ_R for curves of constant rate. This is shown in Fig. 8. For $Q = 200$ [Fig. 8(a)], the maximum SNR occurs around $\sigma_R = 6$; for $Q = 32$ [Fig. 8(b)], the maximum occurs around $\sigma_R = 4$; for $Q = 8$ [Fig. 8(b)], the maximum appears to be between $\sigma_R = 3$ and $\sigma_R = 4$. Table 2 summarizes the turbulence parameters at which capacity is computed for $Q = 200$. We estimate the error in the capacity—assuming the validity of the gamma–gamma model—to be lower than 1%.

5. Efficient LDPC Error-Correction Codes

We have found in the previous section that capacity can be severely reduced with scintillation. Hence, the FSO probability of bit error can be very high, even for large values of SNR [26]. This renders the atmospheric FSO channel useless, as such high SNR is not attainable in practice. Therefore, powerful error-correction codes are necessary. Our analysis will focus on two classes of codes: RS codes and LDPC codes [8, 9, 27]. Some Turbo codes [28] have already been evaluated for use on the FSO channel under weak turbulence [7].

We evaluate two LDPC error-correction codes for the FSO channel that can efficiently operate across all turbulence regimes. These codes were recently proposed for bursty channels, such as fiber-optics channel operating at 40 Gbit/s or higher, outperforming turbo product codes of comparable code rates [8, 9]. The atmospheric FSO channel also shows bursty-error–prone behavior, making these codes appealing for this channel. They also have large minimum distances, have a regular structure, and are designed using the concepts of combinatorial design [10]. These codes also have low encoding and decoding complexity, which is a desirable feature for implementation in actual FSO communication systems. Namely, the quasi-cyclic structure of parity-check matrix of the considered LDPC codes facilitates the implementation, because only the dimension of the permutation matrix and the exponents are to be memorized. For the details of an LDPC chip architecture an interested reader is referred to [29]. The codeword lengths are 2025 bits and 4320 bits long, with rates 0.91 and 0.75, respectively.

Figure 9 shows the BER curves for a turbulence strength of $\sigma_R = 0.6$ (weak turbulence) of the rate 0.91 LDPC, the rate 0.75 LDPC, a rate 0.94 RS (255, 239) code, and a rate 0.75 RS (255, 191) code. The BER of the uncoded system is also depicted. The Shannon limits for rates 0.91 and 0.75 are also plotted and represent the best performance one can achieve

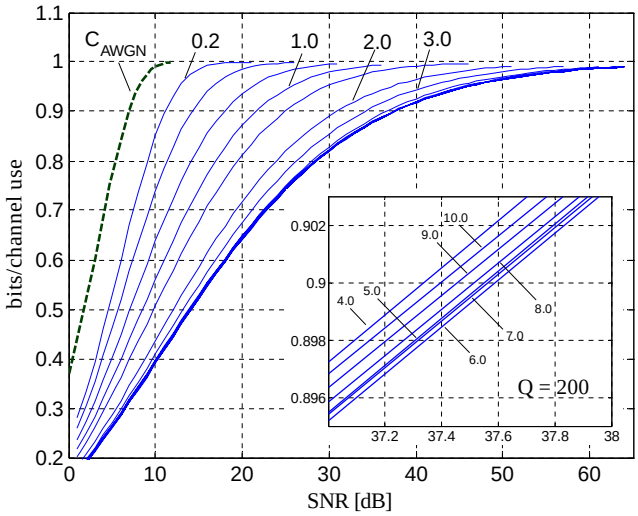

Fig. 5. Capacity versus σ_R versus SNR for $Q = 200$. The inset is a closeup around 37.5 dB.

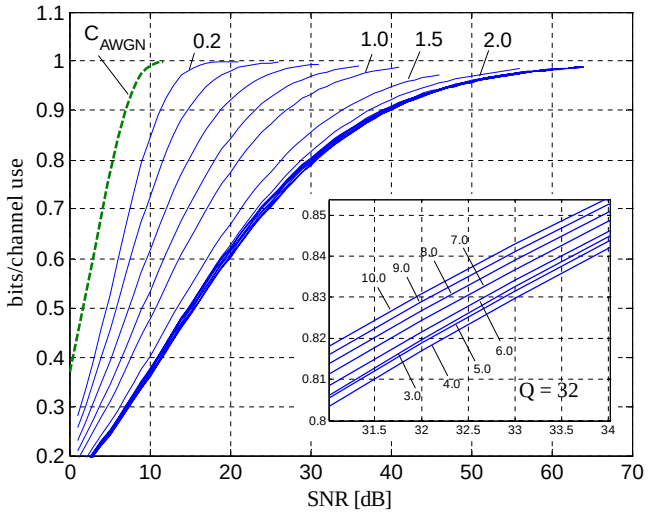

Fig. 6. Capacity versus σ_R versus SNR for $Q = 32$. The inset is a close-up around 32 dB.

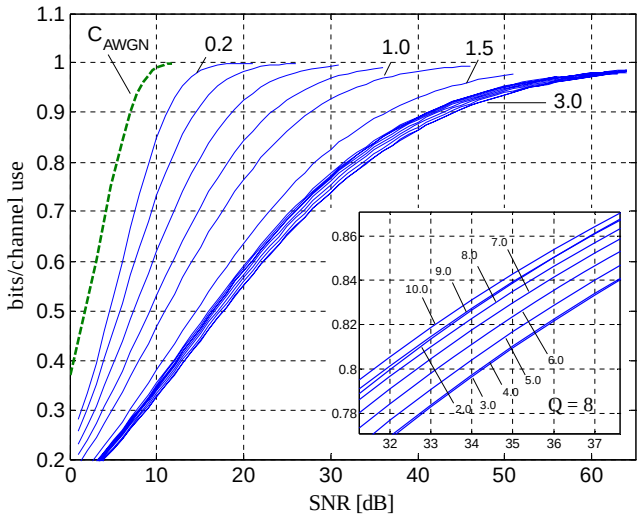

Fig. 7. Capacity versus σ_R versus SNR for $Q = 8$. The inset is a closeup around 34 dB.

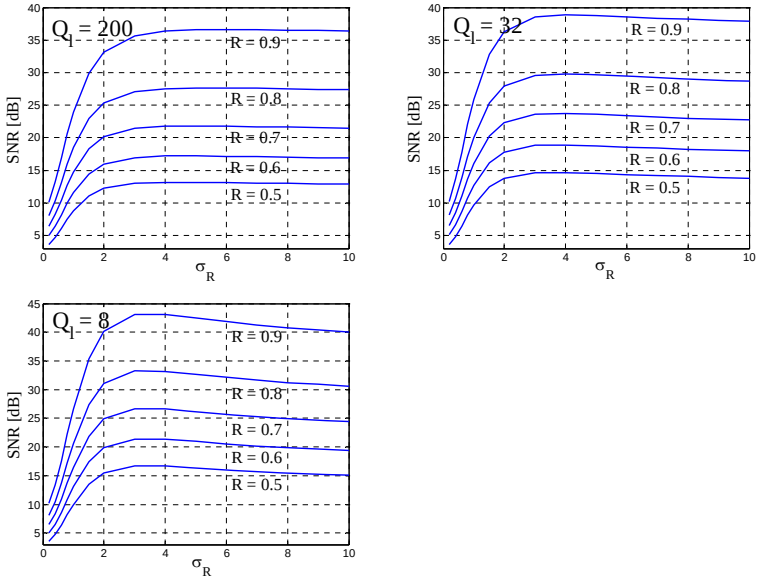

Fig. 8. Required SNR to maintain a constant rate as a function of σ_R, for (a) $Q = 200$, (b) $Q = 32$, and (c) $Q = 8$.

with an infinitely long FEC code. The coding gain of the rate 0.91 LDPC code with respect to the rate 0.94 RS code is 5.5 dB, and the coding gain of the rate 0.75 LDPC code with respect to the rate 0.75 RS code is 6.3 at BER $= 10^{-7}$. The coding gain of the LDPC codes over an uncoded system is more than 20 dB, which is an outstanding improvement, as these coding gains are rarely seen in other channels. The performances of the LDPC codes are 5 dB and 4 dB away from their respective Shannon limits.

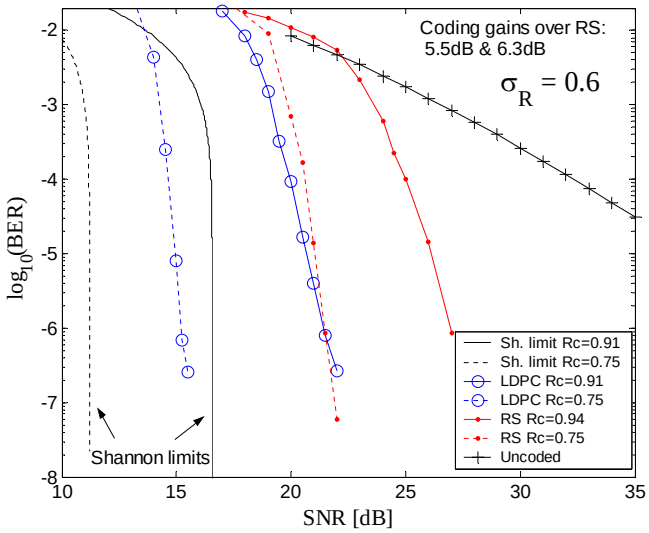

Fig. 9. BER versus SNR for $\sigma_R = 0.6$.

The BER performance for a turbulence strength of $\sigma_R = 0.8$ (weak turbulence) is shown in Fig. 10. The coding gain of the rate 0.91 LDPC code over the rate 0.94 RS (255, 239) code is 6.7 dB. The gain over the uncoded system is again larger than 20 dB, although the whole range is not depicted in Fig. 10. The BER curve of the LDPC code is about 7 dB away from the Shannon limit at BER $= 10^{-7}$.

Figure 11 shows the BER performance of both LPDC codes and both RS codes for a turbulence strength of $\sigma_R = 1.0$. This corresponds to a medium turbulent strength. The coding gains in this case are 7.5 dB and 9.0 dB over the RS codes, respectively. For this turbulence strength, the performance of the uncoded system is so poor that in practice a system cannot operate without coding, because an SNR of 50 dB is almost impossible to achieve.

Figures 12, 13 show the BER performance in the strong turbulence regime for $\sigma_R = 2.0$ and $\sigma_R = 3.0$ respectively. LDPC coding gains with respect to the RS codes are even larger than in previous cases: 10.5 dB and 12 dB for the rate 0.91 code, at $\sigma_R = 2.0$ and $\sigma_R = 3.0$ respectively, and 12 dB and 14 dB respectively for the rate 0.75 codes. The performance of the LPDC codes departs more from the Shannon limit than for weaker turbulence, so there is more room for improvement here. The uncoded channel under this turbulence strength is almost useless. However, the values of capacity presented above show that although the BER performance of these uncoded channels is very poor, there is a significant room for improvement if appropriate channel codes are used, particularly at lower code rates.

6. Conclusions

We analyze the atmospheric FSO channel from the perspective of information theory. This analysis is based on a gamma–gamma distribution model of the scintillation that has been

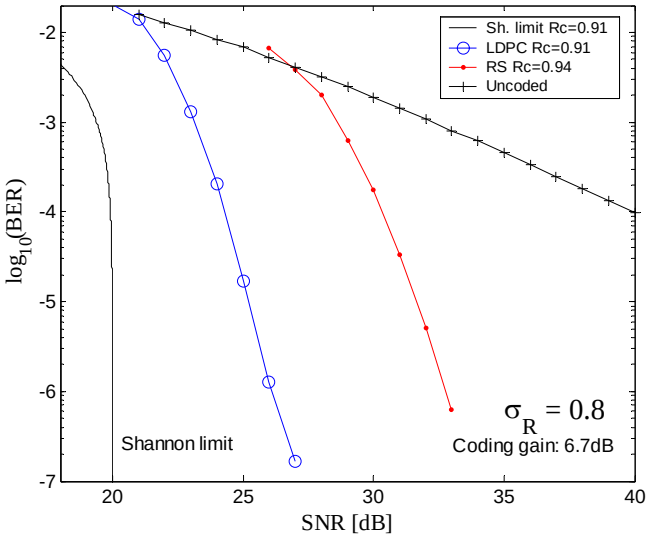

Fig. 10. BER versus SNR for $\sigma_R = 0.8$.

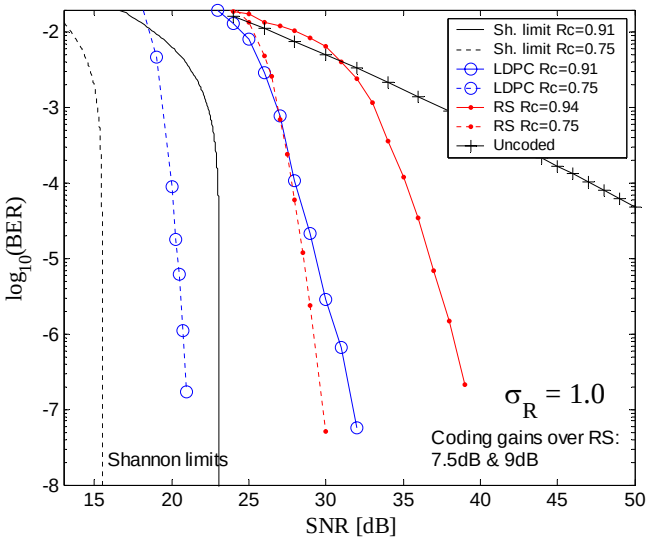

Fig. 11. BER versus SNR for $\sigma_R = 1$.

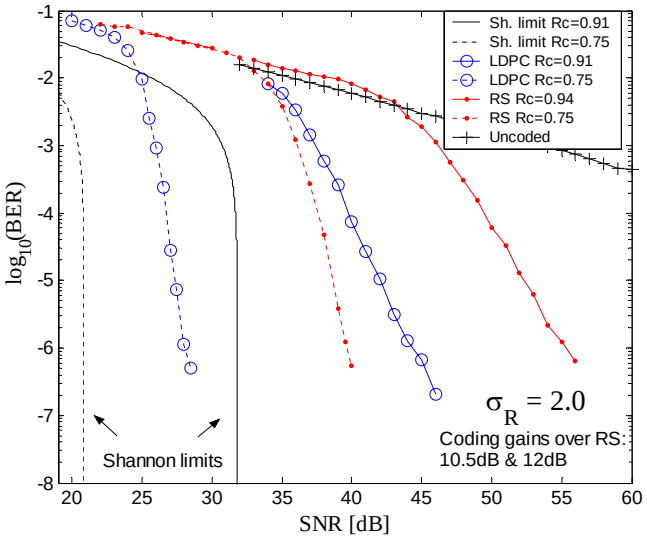

Fig. 12. BER versus SNR for $\sigma_R = 2$.

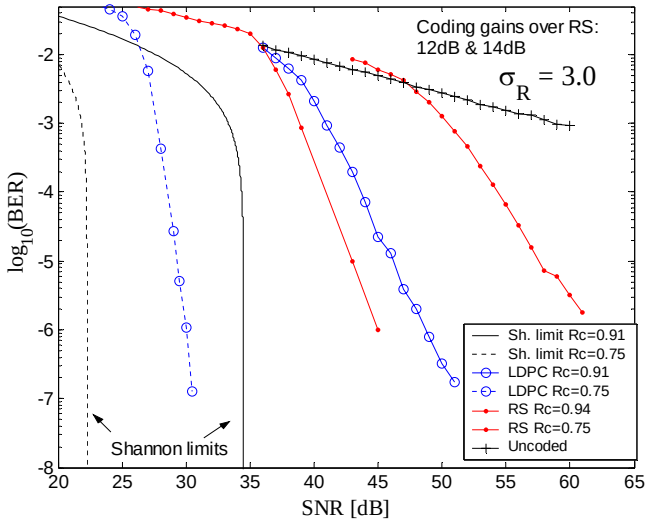

Fig. 13. BER versus SNR for $\sigma_R = 3$.

shown to be a good representation of the actual effect of turbulence. We determine the channel capacity of the atmospheric FSO channel for a point receiver from weak through very strong turbulence conditions. For this analysis we consider both the zero and the nonzero inner scale instances.

We observe that the capacity reduces as the turbulence strength σ_R increases. This reduction is monotonic with σ_R at zero inner scale. We observe that for any given rate, the capacity decreases more rapidly at lower values of σ_R than at higher ones. At non-zero inner scale, we observe that for constant σ_R, the capacity decreases as l_0 increases. We also note that the capacity does not monotonically decrease with σ_R: it begins to grow over a certain value of σ_R, and this increment is more evident as l_0 increases.

We evaluate two error-correction systems based on LDPC codes with excellent correction capabilities for the FSO channel. We show that these codes provide very large SNR gains over Reed–Solomon codes of similar rate for a wide range of turbulence conditions. The delivered coding gains appear to grow as turbulence strengthens. These codes have been designed to provide low encoder and decoder complexity, making them very suitable for practical FSO communication systems.

Acknowledgment

This work is supported by the NSF under grant ITR-00325979.

References and Links

[1] X. Zhu and J. M. Kahn, "Free-space optical communication through atmospheric turbulence channels," IEEE Trans. Commun., **50**, 1293–1300 (2002).

[2] A. C. Boucouvalas, "Guest editorial—Optical wireless communications," IEEE Wireless Commun. **10**, 6–7 (2003).

[3] A. Ishimaru, *Wave Propagation and Scattering in Random Media* (Academic, New York, 1978), Vols. 1–2.

[4] M. A. Al-Habash, L. C. Andrews, and R. L. Phillips, "Mathematical model for the irradiance probability density function of a laser beam propagating through turbulent media," Opt. Eng. **40**, 1554–1562 (2001).

[5] M. Uysal and J. Li, "Error rate performance of coded free-space optical links over gamma-gamma turbulence channels," in *Proceedings of IEEE International Conference on Communication ICC'04* (IEEE, 2004), Vol. 6, pp. 3331-3335.

[6] L. C. Andrews, R. L. Phillips, C. Y. Hopen, M. A. Al-Habash, "Theory of optical scintillation," J. Opt. Soc. Am. A **16**, 1417–1429 (1999).

[7] Jing Li, M. Uysal, , "Achievable information rate for outdoor free space optical communication with intensity modulation and direct detection," in *Global Telecommunications Conference 2003. GLOBECOM '03* (IEEE, 2003), Vol. 5, 2654–2658.

[8] I. B. Djordjevic and B. Vasic, "MacNeish-Mann theorem based iteratively decodable codes for optical communication systems," IEEE Commun. Lett. **8**, 538–540 (2004).

[9] O. Milenkovic, I. B. Djordjevic, and B. Vasic, "Block-circulant low-density parity-check codes for optical communication systems," J. Sel. Top. Quant. Electron. **10**, 294–299 (2004).

[10] B. Vasic, O. Milenkovic "Combinatorial construction of low-density parity check codes," IEEE Trans. Inf. Theory **50**, 1156–1176 (2004).

[11] Y. Kou, S. Lin, M. P. C. Fossorier, "Low-density parity-check codes based on finite geometries: a rediscovery and new results," IEEE Trans. Inf. Theory **47**, 2711–2736 (2001).

[12] L. C. Andrews, R. L. Phillips, and C. Y. Hopen, *Laser Beam Scintillation with Applications* (SPIE, 2001).

[13] S. Karp, R. Gagliardi, S. E. Moran, and L. B. Stotts, *Optical Channels* (Plenum, 1988).

[14] L. C. Andrews and R. L. Phillips, *Laser Beam Propagation through Random Media* (SPIE, 1998).

[15] S. M. Flatté, C. Bracher, and G.-Y. Wang, "Probability-density functions of irradiance for waves in atmospheric turbulence calculated by numerical simulation," J. Opt. Soc. Am. A **11**, 2080–2092 (1994).
[16] L. C. Andrews and R. L. Phillips, "I-K distribution as a universal propagation model of laser beams in atmospheric turbulence," J. Opt. Soc. Am. A **2**, 160–163 (1985).
[17] L. C. Andrews and R. L. Phillips, "Mathematical genesis of the I-K distribution for random optical fields," J. Opt. Soc. Am. A **3**, 1912–1919 (1986).
[18] J. H. Churnside and R. J. Hill, "Probability density of irradiance scintillations for strong path-integrated refractive turbulence," J. Opt. Soc. Am. A **4**, 727–733 (1987).
[19] R. J. Hill and R. G. Frehlich, "Probability distribution of irradiance for the onset of strong scintillation," J. Opt. Soc. Am. A **14**, 1530–1540 (1997).
[20] J. H. Churnside and R. G. Frehlich, "Experimental evaluation of log-normally modulated Rician and IK models of optical scintillation in the atmosphere," J. Opt. Soc. Am. A **6**, 1760–1766 (1989).
[21] T. M. Cover and J. A. Thomas, *Elements of Information Theory* (Wiley-Interscience, 1991).
[22] D. P. Palomar, J. R. Fonollosa, and M. A. Lagunas, "Capacity results of spatially correlated frequency-selective MIMO channels in UMTS," in *54th IEEE Vehicular Technology Conference, 2001. VTC 2001* (IEEE, 2001), Vol. 2, 553–557.
[23] M. Fozunbal, S. W. McLauhlin, R. W. Schafer, "On performance limits of MIMO-OFDM systems over block-fading channels," in *Wireless Communications and Networking Conference, 2004. WCNC* (IEEE, 2004), Vol. 2, 976–980.
[24] A. Papoulis, *Probability, Random Variables, and Stochastic Processes* (WCB/McGraw Hill, 1991).
[25] C. P. Robert, G. Casella, *Monte Carlo Statistical Methods* (Springer-Verlag, 2004).
[26] M. Uysal, S. Mohammad Navidpour, and J. Li, "Error rate performance of coded free-space optical links over strong turbulence channels," IEEE Commun. Lett., **8**, 635–637 (2004).
[27] S. Lin, D. J. Costello, *Error Control Coding* (Prentice Hall, 2004).
[28] W. E. Ryan, "Concatenated convolutional codes and iterative decoding," in *Wiley Encyclopedia in Telecommunications*, J. G. Proakis, ed. (Wiley, 2003).
[29] M. Mansour, "Implementation of LDPC Decoders," presented at the IEEE Comm. Theory Workshop, Park City, Utah, 13–15 June 2005.